Journal of Nuclear Medicine, published on August 12, 2019 as doi:10.2967/jnumed.118.219576

Biodistribution and Dosimetry of Intraventricularly Administered ^{124}I-Omburtamab in Patients with Metastatic Leptomeningeal Tumors

Neeta Pandit-Taskar[1,2], Pat B. Zanzonico[1,3], Kim Kramer[4], Milan Grkovski[3], Edward K. Fung[3], Weiji Shi[5], Zhigang Zhang[5], Serge K. Lyashchenko[6], Alex M. Fung[1], Keith S. Pentlow[3], Jorge A. Carrasquillo[1], Jason S. Lewis[1,2,6], Steven M. Larson[1,7], Nai-Kong V. Cheung[4], John L. Humm[1,3]

[1]Department of Radiology, Memorial Sloan Kettering Cancer Center, New York, NY
[2]Department of Radiology, Weill Cornell Medical College, New York, NY
[3]Department of Medical Physics, Memorial Sloan Kettering Cancer Center, New York, NY
[4]Department of Pediatrics, Memorial Sloan Kettering Cancer Center, New York, NY
[5]Department of Biostatistics & Epidemiology, Memorial Sloan Kettering Cancer Center, New York, NY
[6]Radiochemistry and Molecular Imaging Probe Core, Memorial Sloan Kettering Cancer Center, New York, NY
[7]Molecular Pharmacology Program, Memorial Sloan Kettering Cancer Center, New York, NY

Corresponding Author:
Neeta Pandit-Taskar, MD
Molecular Imaging and Therapy Service, Department of Radiology
Memorial Sloan Kettering Cancer Center
1275 York Avenue, New York, NY 10065
Phone: 212-639-3046; Fax: 212-717-3264; Email: Pandit-n@mskcc.org

Word count: 4,905

Financial support: This research was funded in part through the NIH/NCI Cancer Center Support Grant P30 CA008748.

Running title: ^{124}I-Omburtamab in Leptomeningeal Tumors

ABSTRACT

Radiation dose estimations are key for optimizing therapies. We studied the role of ^{124}I-Omburtamab (8H9) given intraventricularly in assessing the distribution and radiation doses prior to ^{131}I-Omburtamab therapy in patients with metastatic leptomeningeal disease and compared it to the estimates from cerebrospinal fluid (CSF) sampling. **Methods:** Patients with histologically proven malignancy and metastatic disease to the central nervous system or leptomeninges who met eligibility criteria for ^{131}I-Omburtamab therapy underwent immunoPET imaging with ^{124}I-8H9 followed by ^{131}I-8H9 antibody therapy. Patients were imaged with ~74 MBq of intraventricular ^{124}I-Omburtamab via an Ommaya reservoir. Whole-body PET images were acquired at ~4, 24, and 48 h post-administration and analyzed for dosimetry calculations. Peripheral blood and CSF samples were obtained at multiple time points for dosimetry estimation. **Results:** Forty-two patients with complete dosimetry and therapy data were analyzed. ^{124}I- Omburtamab PET-based radiation dosimetry estimations revealed mean ($\pm$ standard deviation) absorbed dose to the CSF for ^{131}I-8H9 of 0.62±0.40 cGy/MBq, compared to 2.22±2.19 cGy/MBq based on ^{124}I-Omburtamab CSF samples, and 1.53±1.37 cGy/MBq based on ^{131}I-Omburtamab CSF samples. The mean absorbed dose to the blood was 0.051±0.11 cGy/MBq for ^{124}I-Omburtamab samples and 0.07±0.04 cGy/MBq for ^{131}I-Omburtamab samples. The effective whole-body radiation dose for ^{124}I-Omburtamab was 0.49±0.27 mSv/MBq. The mean whole-body clearance half time was 44.98±16.29 h. **Conclusion:** PET imaging with ^{124}I-Omburtamab antibody administered intraventricularly allows for noninvasive estimation of dose to CSF and normal organs. High CSF-to-blood absorbed-dose ratios are noted, allowing for improved therapeutic index to leptomeningeal disease and reducing systemic doses. PET imaging-based estimates were less variable and more reliable than CSF sample-based dosimetry.

Keywords: Iodine-124, PET, radioimmunotherapy, cerebrospinal fluid, intraventricular

INTRODUCTION

Central nervous system metastasis is seen in advanced stages of several pediatric as well as adult malignancies including leukemia, neuroblastoma, medulloblastoma, and other solid tumors, and is associated with significant morbidity and high mortality. For patients with high-risk neuroblastoma, incidence of metastatic disease to the central nervous system as well as recurrence is increasing (*1,2*). The cerebrospinal fluid (CSF) space is believed to be a conduit for leptomeningeal spread and a site for metastasis. Intrathecal or intracavitary administration of radiolabeled antibodies has been successfully applied in other malignancies, such as malignant gliomas, with low toxicity and encouraging results (*3,4*). We have previously reported on the use of radioimmunotherapy (*5*) and the feasibility of intrathecal therapy with monoclonal antibodies (*2,6,7*) in neuroblastoma. We have utilized single-photon imaging with the ^{131}I-labeled antibody 3F8, which targets disialoganglioside 2 (GD2)-expressing tumors, for imaging and dosimetry estimations (*6,7*). A murine monoclonal antibody, Omburtamab (8H9), targets the glycoprotein B7-H3 on cell membranes and is expressed in several human solid tumors including neuroblastoma (*8,9*). We evaluated pre-therapy PET imaging with intraventricular injection for estimating radiation doses to CSF in patients with known leptomeningeal disease undergoing treatment with ^{131}I-Omburtamab and compared the PET-based dose estimates with those from CSF sampling.

MATERIALS AND METHODS

This prospective study of ^{124}I-Omburtamab and ^{131}I-Omburtamab imaging and therapy was performed under an institutional review board (IRB)-approved (Clinicaltrials.gov

NCT00089245) and a US Food and Drug Administration-approved Investigational New Drug application BB-IND #9351. All patients or their legal guardians provided written informed consent.

Patients with histologically confirmed diagnosis of a malignancy with Omburtamab reactivity and with evidence of central nervous system /leptomeningeal disease who met all other eligibility criteria for therapy with intra-ventricular ^{131}I-Omburtamab were studied. The characteristics of the study population are presented in Table 1; the study schema is shown in Figure 1. Patients with obstructive or symptomatic communicating hydrocephalus and those who had received cranial or spinal irradiation less than three weeks prior to the start of the protocol were excluded. All patients underwent CSF flow study with ^{111}In-DTPA imaging to ensure the Ommaya reservoir patency and adequate CSF flow. Patients underwent a pre-therapy dosimetry study with ^{124}I-Omburtamab PET imaging, which was used to estimate radiation-absorbed dose to the CSF and normal organs. Subsequently, patients were treated with ^{131}I-Omburtamab within one week at various therapeutic dose levels, as detailed below. Multiple CSF and blood samples were obtained following ^{124}I-Omburtamab administration as well as after therapy with ^{131}I-Omburtamab to estimate radiation dose to CSF and blood. Predicted dosimetry from ^{124}I-Omburtamab and the actual therapeutic ^{131}I-Omburtamab dosimetry was compared.

^{124}I-Omburtamab Radiolabeling

Radiolabeling of ^{124}I-Omburtamab was performed by the Radiochemistry and Molecular Imaging Probes core facility. ^{124}I-Omburtamab was prepared using ~1 mg of the unlabeled antibody and up to 1295 MBq (35 mCi) of ^{124}I (produced by the institutional core facility) with iodogen method, followed by purification with an anion exchange resin and terminal sterilization by microfiltration. Prior to the release for patient administration, the ^{124}I-Omburtamab drug product was tested to ensure radiochemical purity of ≥90%, as determined by thin-layer radiochromatography and immunoreactive fraction determination using a live antigen-expressing cell assay. Sterility testing by media inoculation was performed post-release. Final prepared patient-specific unit doses comprised 74 MBq (2.0 mCi) of ^{124}I-Omburtamab, containing 1.0 mg of the monoclonal antibody, formulated in ~0.8-2.2 mL of ~3-5% (v/v) human serum albumin (HSA) solution in phosphate buffer. The therapeutic antibody's specific activity was 1295-1850 MBq/mg (35-50 mCi/mg).

Administration

Patients were prepared with liothyronine sodium (Cytomel) and saturated solution of potassium iodide (SSKI) to for thyroid protection before infusion of both the ^{124}I dosimetry and ^{131}I therapeutic administrations. Both imaging and treatment dose were given via the Ommaya shunt, accessed using sterile precautions. A baseline CSF sample was drawn for pharmacokinetic analysis (1-2 cc) followed by an additional 2-3 cc of CSF for flush. Following confirmation of a good CSF flow return, the radiolabeled ^{124}I-Omburtamab was injected slowly over ~1 min followed by 1% HSA (~1 cc) and CSF flush (total volume ≤3 cc). The therapeutic dose of ^{131}I-Omburtamab was administered via the Ommaya shunt using the same technique within a week of the imaging study.

Imaging

Three PET scans were performed at approximately 4, 24, and 48 h post-^{124}I-Omburtamab injection. All scans were performed from vertex to pelvis, in 2D mode on a General Electric Discovery PET/CT scanner, using the ^{124}I setting (positron yield: 0.23; physical half-life: 4.18 d) and duration of four minutes per field of view on the day of the radiolabeled antibody administration and five minutes on subsequent imaging days. PET emission data were corrected for attenuation, scatter, and random events, and reconstructed into a 128×128×47 matrix (voxel dimensions: 5.47×5.47×3.27 mm) using the GE ordered subset expectation maximization algorithm with standard clinical reconstruction parameters: 2 iterations, 16 subsets, and a Gaussian post-filter with a full-width at half-maximum of 6.0 mm. Since all PET acquisitions were conducted in 2D mode, no specialized reconstruction software was required to account for "prompt" ^{124}I gamma-ray emissions.

PET Scan-based Dosimetry

VOIs were generated over: liver, salivary glands, spleen, stomach contents, thyroid, and brain for each of the three time-point images using Hermes Hybrid Viewer (Hermes Medical Solutions, Chicago, IL). Whole-body counts were obtained from scanner acquisition data. The VOIs encompassing the entire CSF pool in spinal canal as well as the CSF sub-volumes in lateral ventricles and cervical, thoracic, and lumbar spine were created. CSF and organ time-activity concentration curves were fit to exponential functions and values were decay-corrected for ^{124}I. Areas under the concentration curves were determined by analytical integration to infinity of the fitted exponential functions, incorporating the physical decay of the therapeutic radionuclide ^{131}I to yield the cumulated activity concentrations per unit administered activity of ^{131}I in the CSF and organs. Whole-organ cumulated activities per unit administered activity of ^{131}I were then calculated by multiplying the organ areas under the concentration curves by the corresponding reference organ masses (Oak Ridge National Laboratory) linearly scaled to the respective patient's whole-body mass and used to estimate mean organ-absorbed doses using the OLINDA/EXM software (*10*).

The narrow cylindrical shape and diameters (average 13-15 mm) of the spinal column containing the CSF resulted in an unknown partial-volume error (*11*,*12*). Doses were estimated to entire CSF and four sub-regions (lateral ventricles and cervical, thoracic, and lumbar spine), based on the maximum activity concentration (MBq/cc equivalent to MBq/g assuming unit-density tissue) for each VOI. This was done to investigate possible differences along the length of the spinal column resulting from small occult-disease plaques on the leptomeninges.

The PET data for all regions were fit to a single exponential clearance function, and the curves were integrated to yield a cumulative activity within each of the VOI-defined CSF compartments. Based on their respective physical half-lives, the ^{124}I data were converted to the corresponding data for ^{131}I and multiplied by the equilibrium dose constant for ^{131}I for all electron emission (beta, internal conversion and Auger). We obtained the absorbed doses to the CSF, assuming total local absorption of all electron emissions.

CSF Sample-based Dosimetry

Multiple CSF samples were obtained via the Ommaya access following ^{124}I-Omburtamab dosimetry and ^{131}I-Omburtamab therapeutic administrations, including a baseline sample prior to injection and again at 15±5, 30±5, 60±5, and 120±10 min and 2-4, 18-24, and 42-48 h post-injection. For all samples, an initial 3 cc of CSF was discarded and an additional 1-2 cc was used for assay/counting. Activity in measured CSF aliquots (10 µl) was measured in duplicate using a

NaI (Tl) scintillation well counter (Wallac Wizard 1480 automatic gamma counter, Perkin Elmer) together with appropriate standards. The measured count rates were corrected for background count rate and converted to percent injected activity per gram (% IA/g), decay-corrected to the time of administration. The CSF sample data were fit to a bi-exponential function. The clearance curve Y(t) was multiplied by the exponential decay factor for the projected therapy radionuclide ^{131}I (physical half-life: 8.02 days). Integration of this function provided the cumulated activity concentration of ^{131}I, which, when multiplied by the equilibrium dose constant for all ^{131}I non-penetrating emission (beta, internal conversion, and Auger electrons) (0.405 g.cGy/µCi.h) (*13*), yields the mean absorbed dose to the CSF per unit administered activity of ^{131}I in cGy/MBq. This assumes complete local absorption of the beta particles, internal conversion, and Auger electrons and ignores the much lower gamma-ray dose contribution.

Blood Measurements

Multiple blood samples were obtained, including a baseline sample prior to injection of ^{124}I-Omburtamab at 15±5, 30±5, 60±5, and 120±10 min; 2-4, 18-24, and 42-48 h post-injection. Samples were counted in duplicates in the LKB Wallac^{TM} scintillation well counter, calibrated with a ^{124}I standard and checked for constancy with a ^{68}Ge (271 d) β+ emitting standard. The data were subsequently analyzed similar to the CSF samples.

Statistical Analysis

Statistical analysis was performed to assess whether the radiation doses to the CSF as determined by serial PET VOI analysis were equivalent to those determined from CSF samples. We also examined the ability of ^{124}I-Omburtamab imaging to predict the radiation dose for actual therapeutic ^{131}I-Omburtamab administrations. The analysis was performed on paired samples of CSF and blood obtained from tracer and therapy administrations for each patient.

Wilcoxon signed-rank tests were used to detect shifts of median values between paired observations, and Pearson correlation coefficients were calculated to demonstrate correlations between them. To examine the agreement between paired measurements, Bland-Altman plots were generated. To quantitatively assess the agreement, we computed the intra-class correlation coefficient. Statistical software SAS 9.4 (SAS Institute) and R 3.1.1 (https://www.r-project.org/) with packages *ICC*, *psych,* and *Bland Altman Leh* were used for this analysis. All statistical tests were two-sided and $p<0.05$ was considered statistically significant.

RESULTS

Patients

Forty-two patients underwent dosimetric imaging with ^{124}I-Omburtamab, with 22 patients undergoing a second evaluation of ^{124}I-Omburtamab (Table 1). Patients included those with metastatic neuroblastoma (n=32), medulloblastoma (n=2), sarcoma (n=3), and other (n=5), including ependymoma, rhabdoid tumor, melanoma, choroid plexus tumor and chordoma. The average patient age was 7.5 y (range: 3 mo-42 y) with 26 male and 16 female patients. The mean injected activity of ^{124}I-Omburtamab was 71.4 MBq (range: 48.1-77.7 MBq) (1.93 mCi; range: 1.3-2.1 mCi), and specific activity was 74 MBq/mg (2 mCi/mg). Administered ^{131}I-Omburtamab activities ranged between 1258-2960 MBq (34-80 mCi) with specific activity of 1295-1850 MBq/mg (35-50 mCi/mg).

Biodistribution on PET Images

All patients received an intraventricular injection of ~74 MBq (2 mCi) of ^{124}I-Omburtamab via Ommaya catheter. The PET image quality of the study subjects was good despite the low 37-74 MBq (1-2 mCi) administered activity of the ^{124}I-mAb Omburtamab (Fig. 2). The first image acquired between 2-4 h post-injection showed activity mostly in the ventricles and dispersed in the CSF space along the spinal cord down to the level of the cauda equina by 4 h. Activity distributed in the subarachnoid space along the cerebral convexity was visible at 24 h, with spinal canal activity decreasing by 48 h. PET scans showed variable early distribution in the subarachnoid space and progressive dispersion over the convexity by 24 and 48 h. There was minimal or no activity beyond CSF space and within other organs by 2-4 h post-injection. Systemic distribution with visualization of mild activity in other organs was noted by 24 h that increased at 48 h post-injection with low amounts noted in the liver, spleen, kidney, and bladder as well as minimal thyroid and mild stomach activity noted in some patients (Fig. 2). The uptake in liver showed a slight increase by 48 h. Bladder activity increased with time but remained low due to low systemic activity overall. The thyroid activity decreased by 48 h in most patients. Stomach activity was seen variably, mostly appearing at 24 or 48 h. Activity at the site of injection into Ommaya was always seen; however, the amount varied among patients. This probably affected the CSF clearance and dose calculations.

In three patients, prominent activity persisted up to day 2 at the Ommaya reservoir, indicating poor mixing with the flowing CSF compartment; a second, longer component, consistent with longer biological clearance from the CSF compartment, was seen in these patients. Clearance of activity from the ventricles based on ^{124}I-Omburtamab imaging showed a mean half-life of 9.5 h, ranging up to 18 h in all except two patients, one with a clearance half-life of 26 h and another outlier with a substantially high clearance half-life of 44.4 h (more than four times the average). Mild pooling in the Ommaya or asymmetric activity in the ventricles associated with post-surgical changes and cavities was observed up to 24 h, which decreased or resolved by 48 h in 12 patients. In these patients, CSF clearance half-life ranged from 5.5 to 13.8 h for the second component.

Dosimetry Based on ^{124}I-Omburtamab PET

For ^{124}I-Omburtamab, mean whole-body clearance half-time was 44.98±16.29 h. The whole-body dose was 0.45±0.27 mGy/MBq and the effective dose 0.49±0.27 mSv/MBq. The dosimetry in normal organs (Table 2) showed that the liver received the highest dose of 1.58±1.04 mGy/MBq, followed by normal brain parenchyma, which received an average dose of 1.13±0.55 mGy/MBq. The radiation dose to thyroid was low, averaging 0.58 mGy/MBq.

The biological half-lives and dosimetry estimates for these sub-compartments derived from PET data are presented in Tables 3 and 4. The average clearance half-time for the entire CSF was 9.85 h. The ^{124}I-mAb-Omburtamab dose estimates to CSF in lateral ventricles were 0.620±0.395 cGy/MBq, while those for cervical, thoracic, and lumbar regions ranged from 0.445-0.567 cGy/MBq. The CSF in ventricles received the highest radiation dose of the other spinal canal areas. However, the mean and median doses to the different sub-compartments of the spinal canal did not significantly differ from one another. In one patient, the PET estimate was substantially higher than the mean value, attributed to slow clearance from the right lateral ventricle, which showed intense activity on the day of injection and decreased with time, though persisted partially until 48 h, resulting in an estimated dose of 2.95 cGy/MBq. Radiation doses to other organs besides liver were generally low (Table 2). We recognize, however, that these organ dose estimates are based on limited time-activity data, measured at only three time points out to

~48 hours post-infusion; we therefore also analyzed these data applying a terminal clearance biological half-time of 57 hours to the actual fits of the organ time-activity data. The 57-hour half-time was derived from data for a separate group of patients administered ^{124}I-Omburtamab intracranially for whom whole-body time-activity data were collected out to 6 to 8 days post-administration. The number of time points (4–6) and later time (out to 6 or 8 days) provided confidence in the accuracy of the 57-hour clearance half-time. These ^{124}I-Omburtamab time-activity data followed a mono-exponential (single half-time) function. When this clearance half-time was applied to the fitted functions of a subset of our cohort of ^{131}I-Omburtamab patients for whom the dosimetry is presented in Table 2, these revised absorbed-dose estimates for stomach wall, spleen, and liver were only 20 to 30% greater than our original dose estimates. For all other organs, the difference between the original and revised absorbed-dose estimates was <5%.

CSF Pharmacokinetics and Dosimetry from CSF Sample Counts

The CSF clearance was biexponential with initial half-life averaging less than one hour, followed by a longer second half-life, likely more appropriately represents the rate of clearance of the radiolabeled antibody from the CSF compartment. The mean 25%, 59% (median), and 75% quartile biological half-lives for ^{124}I clearance are given in Table 3. Most of the patients exhibited CSF clearance half-lives of less than 24 h, but three cases exhibited much longer half-lives (35-46 h), likely due to slower clearance from the Ommaya reservoir and ventricles as noted on the images. Estimates for various age groups in children showed similar values (Table 3).

The estimate for ^{131}I-Omburtamab doses as derived from ^{124}I-Omburtamab CSF samples was 2.25±0.4 cGy/MBq, while that from actual ^{131}I-Omburtamab therapy was 1.53±1.44 cGy/MBq (Table 4). Overall doses were highly variable. In 9 patients, the dose estimates ranged between

4.42 and 8.44 cGy/MBq, about 2-4 times higher than the average for all. In another patient, the estimated dose was 10.1 cGy/MBq, based on extrapolation from limited sampling (only at 18 h due to logistical limitations). In 7 of these 10 infusions, a very slow clearance (practically zero in three patients) was noted over the initial 8 h; imaging in these patients showed high activity within ventricles and Ommaya up to 48 h imaging.

Blood Dosimetry Data from Sample Counts

The mean and median radiation dose estimates to the blood from ^{131}I-mAb-Omburtamab and those derived from ^{124}I-mAb-Omburtamab are 0.051 cGy/MBq (1.87 cGy/mCi) and 0.039 cGy/MBq (1.44 cGy/mCi), respectively (Table 5). The estimates to blood are higher for the therapy than pre-therapy tracer samples, a possible consequence of the slower clearance of the larger administered mass of antibody for the therapeutic administration.

Statistical Analysis

A total of 50 dose estimates of ^{124}I-^{131}I-Omburtamab were analyzed. A Wilcoxon signed-rank test comparing the doses from intraventricular ^{124}I-Omburtamab PET data from ventricles (D_{PET}) versus ^{124}I-Omburtamab CSF sample data ($D_{samples}$) post-intraventricular administration showed a significant difference between the two measures in terms of the median difference in distribution (p-value < 0.0001). The Pearson correlation coefficient was 0.00655 (p-value: 0.96), indicating no correlation between the two values (Fig. 3A). In most patients, sample-based estimates of activity concentrations were higher than the PET-based estimates and in only three patients were the PET-based estimates was greater than the sample-based estimate. This result is further illustrated by the Bland-Altman analysis (Fig. 3B). In the Bland-Altman plot, each point represents the difference (D_{PET} - $D_{samples}$) on the y-axis versus the average (D_{PET} + $D_{samples}$)/2) on the x-axis for an individual patient. The Bland-Altman plot shows a systematic increase in the difference between the PET versus sample dosimetry estimates with increasing magnitude of the averaged values. This bias is likely a consequence of the higher CSF sample values being associated with slower mixing with the CSF compartment.

For CSF sample data from pre-treatment ^{124}I-Omburtamab and ^{131}I-Omburtamab post-treatment samples, the Wilcoxon signed-rank test showed significant differences (p-value: 0.013) and the Pearson correlation coefficient was 0.084 with a p-value of 0.52, indicating no correlation (Fig. 3C). However, as expected, the paired samples are almost equally distributed about the line of identity, suggesting no systematic difference between the two sample-based dose estimates.

DISCUSSION

Intraventricular infusions of therapeutic agents allow for treating compartmentalized disease while limiting systemic toxicity. To optimize therapeutic outcome, understanding the kinetics and dosimetry of the therapeutic agent is essential. Multiple CSF sampling either directly via lumbar puncture or access catheter such as Ommaya system, allows for direct measurement of the radioactivity, but is invasive with a risk of infection and can be limiting in children. We evaluated the feasibility and utility of ^{124}I-Omburtamab PET imaging for estimating the projected dose for ^{131}I-Omburtamab therapy administered intraventricularly.

With ^{124}I/^{131}I-Omburtamab injected directly into the CSF compartment there was higher activity concentrations within the CSF space with low activity elsewhere during the imaging times, the image quality and target-to-background contrast of ^{124}I-Omburtamab were excellent. The antibody clearance is slow, as visualized by the sequential PET images, allowing for longer duration of radiation exposure to the CSF space and leptomeninges. The dose-limiting toxicity from intravenous administration of radiolabeled antibody therapy is from bone marrow toxicity (typically 200 cGy limit). The relative CSF-to-blood dose ratios are extremely high, ranging between 10-fold for PET-based values to 30-45 for CSF sample-based estimates. Our data suggest that an administered activity of ~4,000 MBq of ^{131}I-Omburtamab could be administered before exceeding a blood dose of 200 cGy. Therefore, even at treatment doses of 1850-2960 MBq (50-80 mCi) given intraventricularly, the blood dose is well below the generally accepted safe limit; thus, no significant marrow toxicity is generally seen.

Our data indicate a wide variation in doses estimated from CSF samples (Table 4). This is likely due to the retrieval technique of CSF samples from the same Ommaya port into which the radiolabeled antibody was injected, where pooling of activity in the reservoir is present, as noted in imaging. In contrast, far less variation was noted with PET imaging-based estimates where the activity in the Ommaya that generates high counts can be and was excluded from the PET VOI ventricle estimates. This also explains the consistently lower PET-based estimates as compared to CSF sample derived estimates. The dose estimates to the different CSF sub-regions was more consistent. Only in a single patient did we observe substantial activity retained in the lateral ventricle on PET images; this was attributed to disease and treatment changes. In this patient, the PET estimate of CSF activity concentration was higher than that measured in CSF samples; this patient exhibited prominent ventricular retention likely related to disease.

We found no significant statistical correlation between CSF sample-based and PET-based estimates. Overall, the radiation dose estimates from ^{124}I CSF sample data was much greater than from the PET data: 2.36 versus 0.63 cGy/MBq, a ratio of 3.74. While in a small group of patients there was agreement between the PET and sample-based dose estimates, the majority showed greater variation. Therefore, dosimetry estimates based on Ommaya samples were found to be less reliable than image-based methods. This is further underscored by the statistical analysis comparing the pre-therapy ^{124}I-Omburtamab CSF sample data versus post-therapy ^{131}I-Omburtamab CSF data, where no significant correlation was found (Fig. 3C). Additionally, while differences in the clearance time and dosimetry noted for pre-therapy versus post-therapy estimates could in part reflect the differing mass amounts of antibody administered, the lack of significant bias does not support this.

The limitations of this study include the comparison of CSF sampling data, which is affected by the technique of sampling (i.e., from the same port into which the radiolabeled antibody was injected). This is a limitation, especially in children, where a separate CSF draw from lumbar puncture at each time point is impractical. Noninvasive imaging methods are therefore preferred. A general practical limitation to ^{124}I imaging is the expense. An alternative approach may be to use dose estimates based on serial gamma camera scans and SPECT imaging with ^{131}I-Omburtamab, though quantitation of single-photon activity remains less reliable in routine clinical practice than that of positron-emitting radionuclides.

CONCLUSION

^{124}I-Omburtamab PET imaging is a noninvasive method to obtain dosimetry estimates in patients undergoing intraventricular therapy with ^{131}I-Omburtamab. ^{124}I-Omburtamab PET imaging dosimetry estimation shows less variation as compared to the estimates by CSF sampling.

Research Funding

This research was funded in part through the NIH/NCI Cancer Center Support Grant P30 CA008748.

Disclosures

N. Pandit-Taskar has served as a consultant to Y-mAbs Therapeutics, Inc., Fluoropharma, and ImaginAb, Inc. and has served on the advisory board of Progenics. She has received honoraria from MedImmune/AstraZeneca. M. Grkovski and E. Fung received support from Y-mAbs Therapeutics, Inc. to perform the normal organ dosimetry from the PET imaging data. S. Lyashchenko reports personal fees from Y-mAbs Therapeutics, Inc. outside the submitted work. J. Carrasquillo has served as a consultant for Y-mAbs Therapeutics, Inc. and Bayer, and has received research funding from Genentech, Inc.; Regeneron Pharmaceuticals, Inc.; and Gilead Sciences, Inc. With regard to this publication, J.S. Lewis's laboratory has received research support from ImaginAb, Inc. S. Larson reports receiving commercial research grants from Genentech, Inc., WILEX AG, Telix Pharmaceuticals Limited, and Regeneron Pharmaceuticals, Inc.; holding ownership interest/equity in Voreyda Theranostics Inc. and Elucida Oncology Inc., and holding stock in ImaginAb, Inc. He is the inventor and owner of issued patents both currently unlicensed and licensed by MSK to Samus Therapeutics, Inc. Elucida Oncology, Inc., and Y-mAbs Therapeutics, Inc. He is or has served as a consultant to Cynvec LLC, Eli Lilly & Co., Prescient Therapeutics Limited, Advanced Innovative Partners, LLC, Gerson Lehrman Group, Progenics Pharmaceuticals, Inc., and Janssen Pharmaceuticals, Inc. N.K. Cheung reports receiving commercial research grants from Y-mAbs Therapeutics, Inc. in 2015 and Abpro-Labs, Inc. in 2017, holding ownership interest/equity in Y-mAbs Therapeutics and in Abpro-Labs, and owning stock options in Eureka Therapeutics, Inc. He is the inventor and owner of issued patents licensed by MSK to Y-mAbs Therapeutics, Biotec Pharmacon, and Abpro Labs. He is a scientific advisory board member of Abpro Labs and Eureka Therapeutics, and is named as an inventor on several patent applications related to GPA33 filed by MSK. No other potential conflicts of interest relevant to this article exist.

KEY POINTS

Question: Does PET imaging of intrathecally administered ^{124}I-Omburtamab add value to the dosimetric estimates for ^{131}I radioimmunotherapy of leptomeningeal disease?

Pertinent Findings: PET imaging provides more robust kinetic and biodistribution data than CSF sampling and overcomes artifact-related errors associated with CSF sampling.

Implications for Patient Care: PET imaging complements CSF analysis and can allow for more optimal estimates through combined analysis and imaging assessment.

REFERENCES

1. Kramer K, Kushner B, Heller G, Cheung NK. Neuroblastoma metastatic to the central nervous system. The Memorial Sloan Kettering Cancer Center experience and a literature review. *Cancer.* 2001;91:1510-1519.

2. Kramer K, Kushner BH, Modak S, et al. Compartmental intrathecal radioimmunotherapy: results for treatment for metastatic CNS neuroblastoma. *J Neurooncol.* 2010;97:409-418.

3. Akabani G, Reardon DA, Coleman RE, et al. Dosimetry and radiographic analysis of 131I-labeled anti-tenascin 81C6 murine monoclonal antibody in newly diagnosed patients with malignant gliomas: a phase II study. *J Nucl Med.* 2005;46:1042-1051.

4. Bigner DD, Brown MT, Friedman AH, et al. Iodine-131-labeled antitenascin monoclonal antibody 81C6 treatment of patients with recurrent malignant gliomas: phase I trial results. *J Clin Oncol.* 1998;16:2202-2212.

5. Cheung NK, Kushner BH, Cheung IY, et al. Anti-G(D2) antibody treatment of minimal residual stage 4 neuroblastoma diagnosed at more than 1 year of age. *J Clin Oncol.* 1998;16:3053-3060.

6. Kramer K, Cheung NK, Humm JL, et al. Targeted radioimmunotherapy for leptomeningeal cancer using (131)I-3F8. *Med Pediatr Oncol.* 2000;35:716-718.

7. Kramer K, Humm JL, Souweidane MM, et al. Phase I study of targeted radioimmunotherapy for leptomeningeal cancers using intra-Ommaya 131-I-3F8. *J Clin Oncol.* 2007;25:5465-5470.

8. Modak S, Kramer K, Gultekin SH, Guo HF, Cheung NK. Monoclonal antibody 8H9 targets a novel cell surface antigen expressed by a wide spectrum of human solid tumors. *Cancer Res.* 2001;61:4048-4054.

9. Xu H, Cheung IY, Guo HF, Cheung NK. MicroRNA miR-29 modulates expression of immunoinhibitory molecule B7-H3: potential implications for immune-based therapy of human solid tumors. *Cancer Res.* 2009;69:6275-6281.

10. Stabin MG, Sparks RB, Crowe E. OLINDA/EXM: the second-generation personal computer software for internal dose assessment in nuclear medicine. *J Nucl Med.* 2005;46:1023-1027.

11. Morishita Y, Naito M, Hymanson H, Miyazaki M, Wu G, Wang JC. The relationship between the cervical spinal canal diameter and the pathological changes in the cervical spine. *Eur Spine J.* 2009;18:877-883.

12. Lee HJ, Kim JT, Shin MH, Choi DY, Hong JT. Quantification of pediatric cervical spine growth at the cranio-vertebral junction. *J Korean Neurosurg Soc.* 2015;57:276-282.

13. Eckerman KF, Endo A. MIRD radionuclide data and decay schemes, 2nd ed. Society of Nuclear Medicine: Reston, VA, 2008.

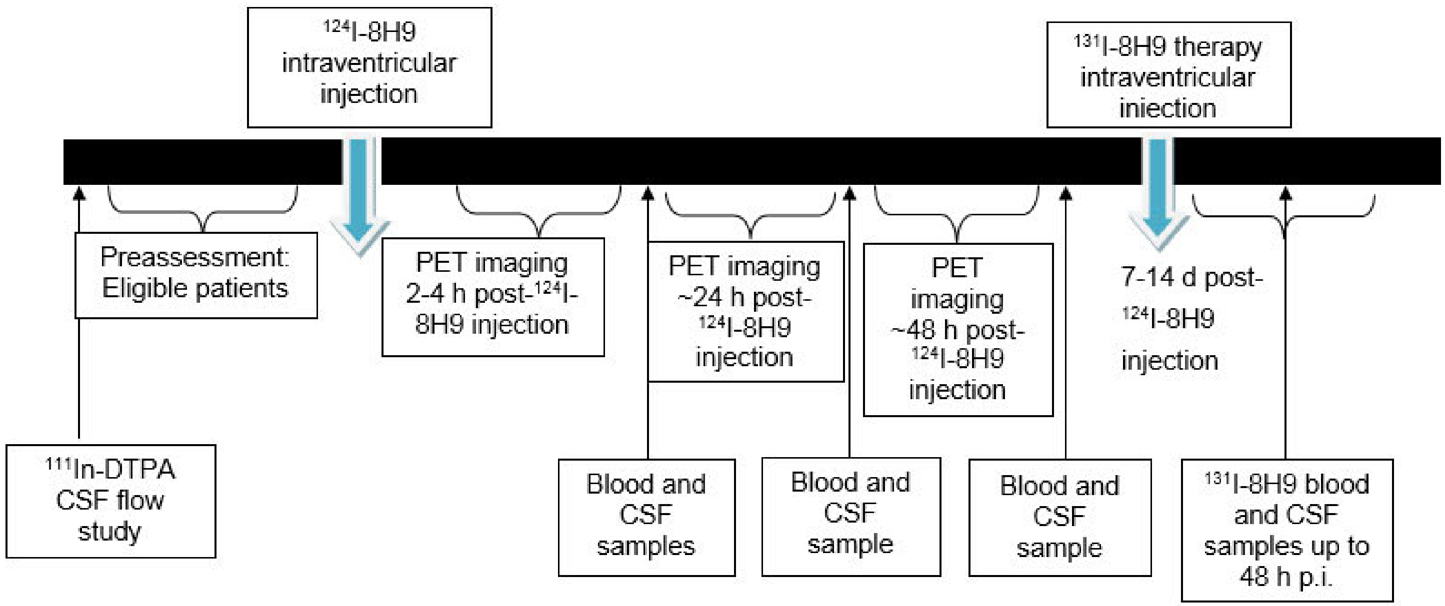

Figure 1. Study schema.

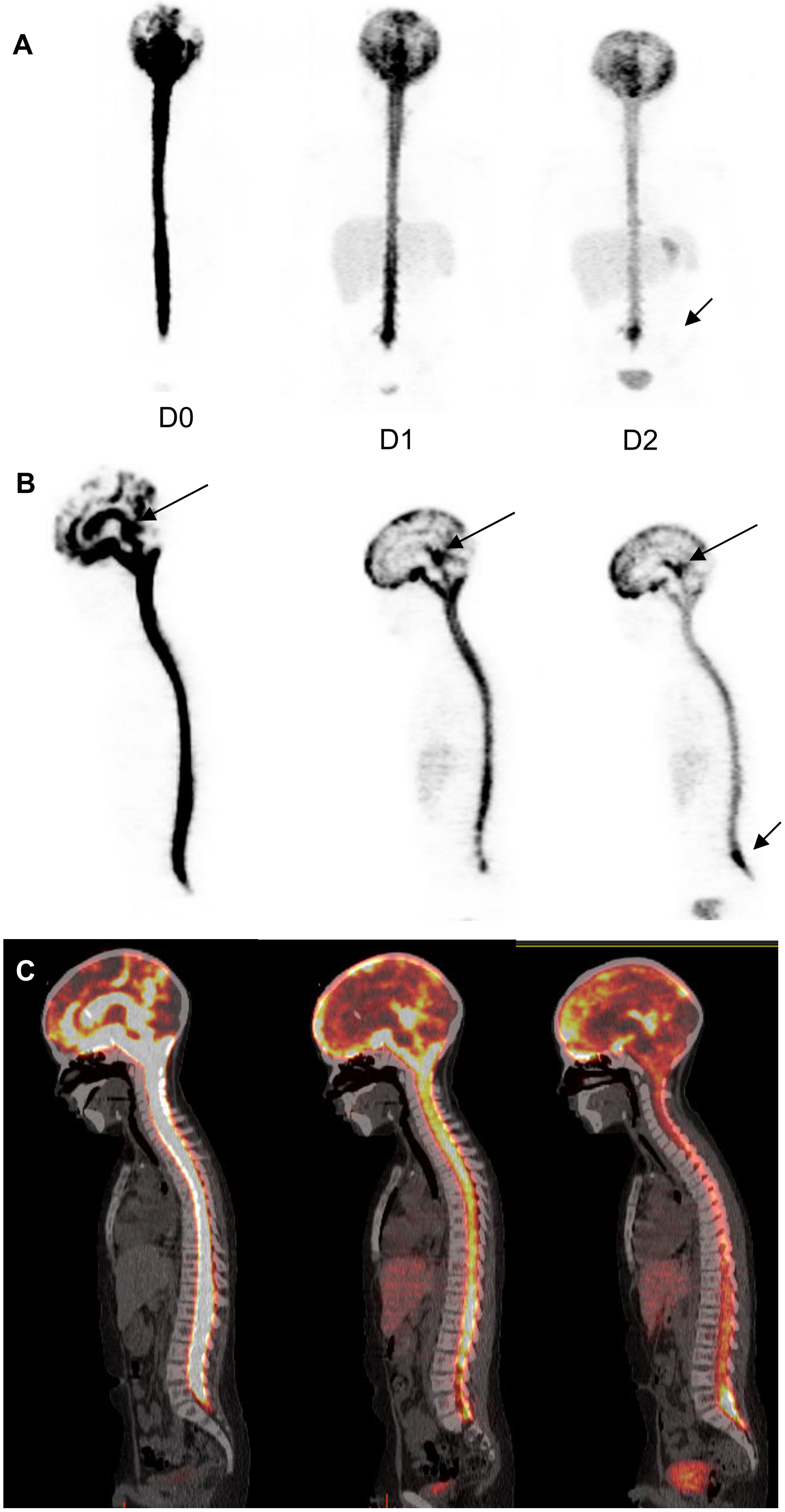

A
D0
D1
D2
B
C

Figure 2. Patient with metastatic neuroblastoma with leptomeningeal disease. Serial ^{124}I-Omburtamab images – MIP (anterior projection) (A); sagittal projection, PET only (B); and fused images (C) from D0, D1, D2 (left to right) show activity within the ventricles and CSF canal that decreases over time. Systemic activity is seen in the liver and bladder in D1 and D2 images. Slower clearance is noted from ventricles in this patient (arrows in B). Pooling is also seen along the cauda equina (short arrow).

A

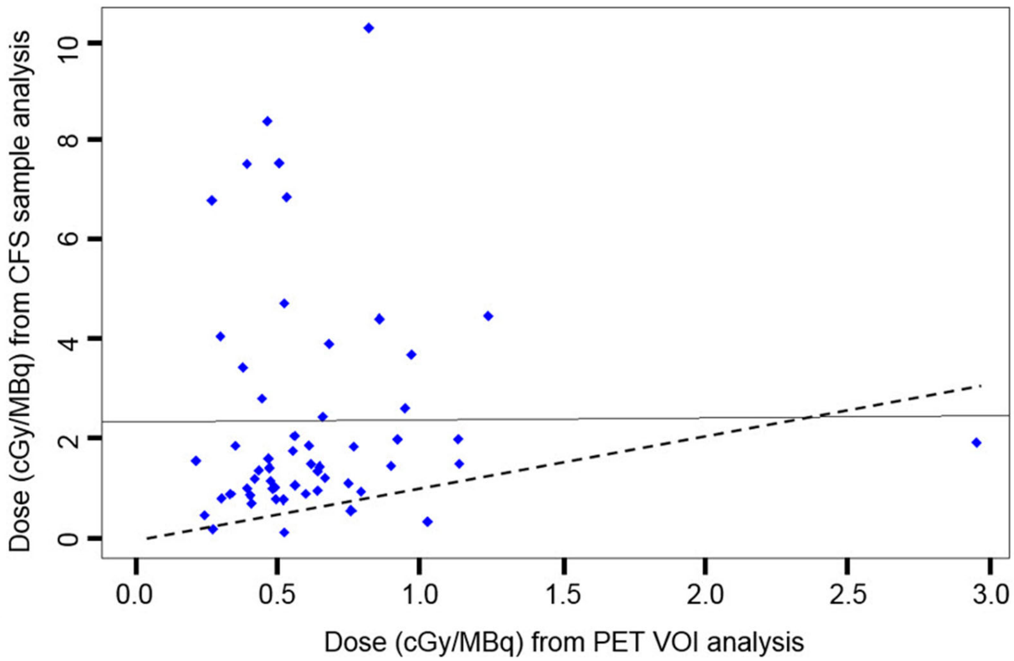
Dose (cGy/MBq) from CFS sample analysis
0
2
4
6
8
10
0.0
0.5
1.0
1.5
2.0
2.5
3.0
Dose (cGy/MBq) from PET VOI analysis

B

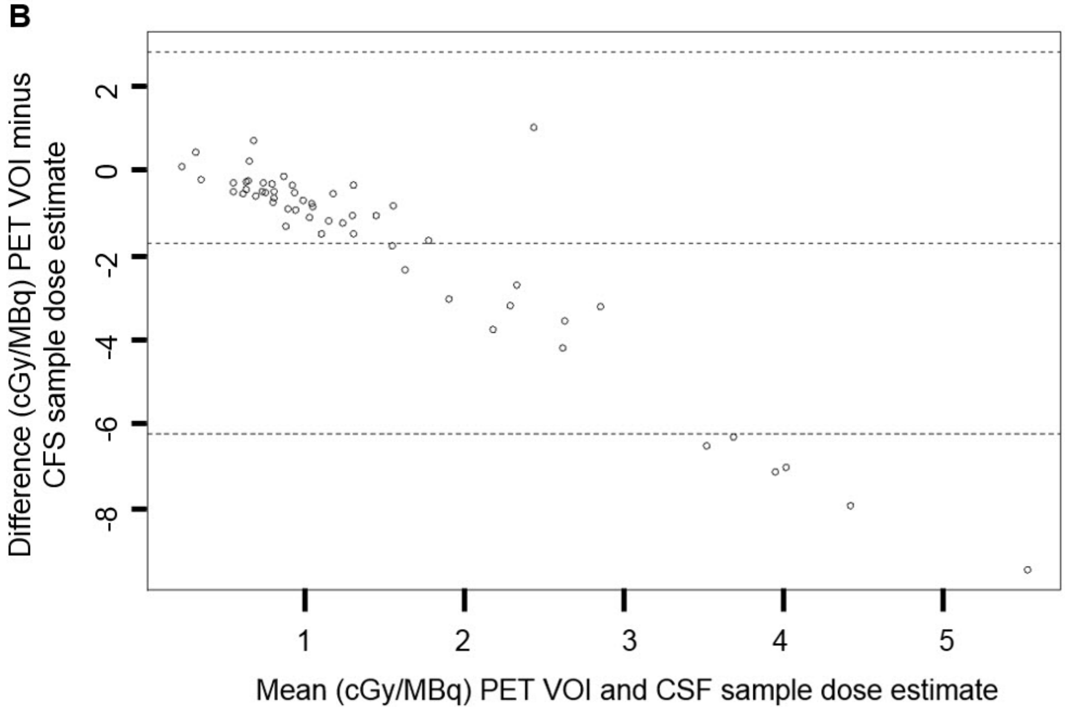
Difference (cGy/MBq) PET VOI minus
CFS sample dose estimate
2
0
-2
-4
-6
-8
1
2
3
4
5
Mean (cGy/MBq) PET VOI and CSF sample dose estimate

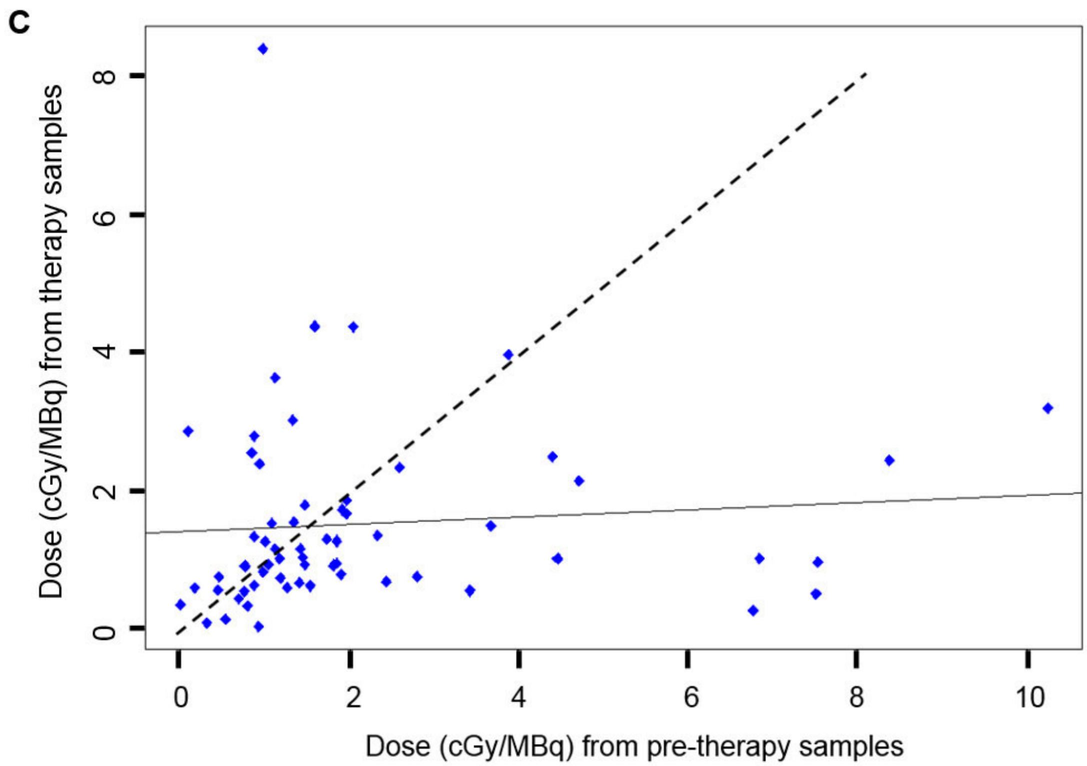

Figure 3. CSF dose estimates for ^{131}I Omburtamab: ^{124}I-Omburtamab PET estimates versus actual ^{124}I- Omburtamab CSF samples (A). Scatter plot showing estimated radiation doses for ^{131}I-Omburtamab in units of cGy/MBq. The x-axis shows dose values estimated from ^{124}I-8H9 PET ROI data versus doses estimated from ^{124}I-8H9 CSF sample counts on the y-axis. The Pearson correlation coefficient was calculated to show the correlation between PET ROI versus sample count data. This coefficient is 0.00655 with a p-value of 0.96, indicating no correlation. The solid and dashed lines represent the lines of correlation and identity, respectively. Bland-Altman plot showing the mean difference between the PET ROI dose and the CSF sample-based dose estimates on the y-axis versus the average of the two dose estimates on the x-axis (B). The 95% confidence intervals for the mean difference was determined using the R package "*Bland Altman Leh*". Scatter plot comparing radiation doses (cGy/MBq) from post-therapy ^{131}I-Omburtamab samples (y-axis) versus the pre-therapy ^{124}I-Omburtamab samples (x-axis) (C). The Pearson coefficient is 0.084 with a p-value of 0.52, indicating no correlation. The solid and dashed lines represent the lines of correlation and identity, respectively.

Table 1. Patient Demographics

Total number of patients	42
Dose (1 only)	20
Dose (2)	22
Primary malignancy – Number of patients	
Neuroblastoma	32
Medulloblastoma	2
Sarcoma	3
Ependymoma	1
Rhabdoid tumor	1
Melanoma	1
Chordoma	1
Choroid plexus tumor	1
Age	3 months-42 y
Sex	
Male	26
Female	16

Table 2. Normal organ-absorbed dose and effective dose estimates for ^{124}I-Omburtamab administered intraventricularly. Units are mGy/MBq unless otherwise noted.

	Mean	SD	Median	Min	Max
Salivary Gland	0.52	0.33	0.44	0.05	1.45
Adrenals	0.41	0.23	0.40	0.06	1.10
Brain	1.13	0.55	1.01	0.20	3.03
Gall bladder wall	0.46	0.24	0.46	0.07	1.13
Lower large intestine Wall	0.36	0.22	0.34	0.06	1.02
Small intestine	0.40	0.24	0.38	0.06	1.02
Stomach wall	0.86	0.57	0.71	0.17	2.65
Upper large intestine wall	0.40	0.23	0.39	0.06	1.08
Heart wall	0.39	0.23	0.37	0.06	1.06
Kidneys	0.39	0.22	0.38	0.06	1.05
Liver	1.58	1.04	1.62	0.06	4.22
Lungs	0.36	0.21	0.34	0.05	1.00
Muscle	0.34	0.21	0.31	0.05	0.98
Pancreas	0.44	0.25	0.44	0.07	1.16
Red marrow	0.37	0.27	0.30	0.05	1.21
Osteogenic cells	0.67	0.43	0.59	0.12	1.99
Skin	0.30	0.18	0.27	0.05	0.85
Spleen	0.57	0.32	0.55	0.04	1.16
Thymus	0.35	0.21	0.32	0.05	0.99
Thyroid	0.58	0.74	0.40	0.07	5.29
Urinary bladder wall	0.35	0.21	0.34	0.06	0.98
Total body	0.45	0.27	0.45	0.07	1.22
Effective Dose (mSv/MBq)	0.49	0.27	0.47	0.10	1.23
Effective Dose Equivalent (mSv/MBq)	0.55	0.28	0.53	0.10	1.32

Table 3. PET imaging and CSF-derived biological clearance half-lives of ^{124}I-Omburtamab from the CSF. Clearance data are presented as the mean, 25%, 50%, and 75% quartiles and the range.

	Median	**25% Q**	**50% Q**	**75% Q**	**Range (h)**	**Mean**			**Median**		
^{124}I-Omburtamab PET	**All**	**All**	**All**	**All**	**All**	**<5 Y**	**5-10 Y**	**>10 Y**	**<5 Y**	**5-10 Y**	**>10 Y**
Ventricle	8.19	6.61	8.89	9.57	3.6-18.2	9.22	8.62	8.81	8.14	8.3	9.01
Cervical	6.86	6.36	9.08	8.89	3.9-16.9	8.13	9.72	9.54	6.78	6.65	9.7
Thoracic	7.83	6.71	11.01	10.39	5.0-25.0	9.14	12.84	10.82	7.51	7.94	9.87
Lumbar	7.02	6.32	9.84	11.05	4.1-39.6	9.46	9.46	14.91	6.62	6.94	11.47
^{124}I-Omburtamab samples	6.3	5.49	10.31	11.63	3.7-46.2	10.15	9.33	9.31	8.41	6.62	5.74

Notes: Excludes outliers 26 h and 44.4 h in a single patient each. 50% quartile: mean all. Q: quartile; h: hours

Table 4. Radiation dose estimates to the CSF for ^{131}I-mAb Omburtamab. Data are presented as the mean dose, 25%, 50%, and 75% quartiles and the range.

		Mean (cGy/MBq)	25% Quartile	Median (cGy/MBq)	75% Quartile	Range (cGy/MBq)
^{124}I-Omburtamab PET-derived doses	Ventricle	0.620	0.436	0.523	0.755	0.21 – 2.948
	Cervical	0.445	0.326	0.387	0.494	0.170 – 0.711
	Thoracic	0.538	0.373	0.442	0.555	0.189 – 1.978
	Lumbar	0.567	0.454	0.552	0.652	0.235 – 1.051
	Whole CSF					
From ^{124}I-Omburtamab CSF samples		2.253	0.961	1.443	2.512	0.100 – 10.243
From ^{131}I-Omburtamab post-therapy CSF samples		1.534	0.695	1.1	1.841	0.041 - 8.386

Table 5. Blood dosimetry estimates for ^{131}I-mAb Omburtamab derived from the pre-therapy ^{124}I-Omburtamab administration and actual ^{131}I-Omburtamab therapy.

	Mean dose (cGy/MBq)	Median dose (cGy/MBq)	Dose range (cGy/MBq)
^{124}I Omburtamab blood samples	0.051	0.039	0.0035 – 0.244
^{131}I Omburtamab blood samples	0.068	0.069	0.0032 – 0.158